Published in final edited form as:

Gastroenterology. 2023 June ; 164(7): 1137–1151.e15. doi:10.1053/j.gastro.2023.02.030.

Stiffness Restricts the Stemness of the Intestinal Stem Cells and Skews Their Differentiation Towards Goblet Cells

Shijie He[1,2,3,4,*], **Peng Lei**[1,2,3,4,*], **Wenying Kang**[5], **Priscilla Cheung**[4,6], **Tao Xu**[4,7], **Miyeko Mana**[8], **Chan Young Park**[9], **Hongyan Wang**[1,4], **Shinya Imada**[8], **Jacquelyn O. Russell**[4,6], **Jianxun Wang**[1,2,3,4], **Ruizhi Wang**[10], **Ziheng Zhou**[1,2,3,4], **Kashish Chetal**[4,11], **Eric Stas**[4,12], **Vidisha Mohad**[1,4], **Peter Bruun-Rasmussen**[13], **Ruslan I. Sadreyev**[4,11,14], **Richard A. Hodin**[1,4], **Yanhang Zhang**[10], **David T. Breault**[4,12,15], **Fernando D. Camargo**[4,6,15], **Ömer H. Yilmaz**[8], **Jeffrey J. Fredberg**[9], **Nima Saeidi**[1,2,3,4,15]

[1]Division of Gastrointestinal and Oncologic Surgery, Department of Surgery, Massachusetts General Hospital, Boston, MA 02114, USA

[2]Center for Engineering in Medicine and Surgery, Department of Surgery, Massachusetts General Hospital, Boston, MA 02114, USA

[3]Shriners Hospital for Children – Boston, MA 02114, USA

[4]Harvard Medical School, Boston, MA 02115, USA

[5]Deparment of Otolaryngology- Head and Neck Surgery, Stanford Medical School, CA 94305, USA

[6]Stem Cell Program and Department of Hematology/Oncology, Children's Hospital, Boston, MA 02115, USA

[7]Section on Pathophysiology and Molecular Pharmacology, Joslin Diabetes Center, Boston, MA 02115, USA

[8]Koch Institute for Integrative Cancer Research, Massachusetts Institute of Technology, Cambridge, MA 02142, USA

[9]Department of Environmental Health, Harvard T.H. Chan School of Public Health, Boston, MA 02115, USA

Correspondence and requests for materials should be addressed to N.S. (nsaeidi@mgh.harvard.edu).

*Shijie He and Peng Lei contributed equally.

Author Contributions S.H. and N.S. conceptualized the work and designed the experiments. S.H. and P.L. performed the experiments with inputs from J.W., P.C., J.O.R. and F.D.C. on generating transgenic mice, C.Y.P. and J.J.F. for live cell imaging, M.M. and Ö.H.Y. for flow cytometry, E.S. and D.T.B for training, and S.I. for in situ hybridization. S.H., H.W. and V.M. performed the DSS mouse model with inputs from Z.Z. for measuring thickness, and R.W. and Y.Z. for measuring stiffness. W.K., K.S., T.X. and P.B. performed the scRNAseq analysis for human and organoids with guidance from S.H., R.S. and N.S. S.H. and N.S. wrote the manuscript. J.J.F., F.D.C., P.C., M.M., C.Y.P., D.T.B., T.X., M.H. and I.A. commented on the manuscript.

The authors declare no competing financial interests. N.S. and S.H. are inventors on a patent application filed based on this investigation.

Data Statement: The processed sc-RNA-seq data of the mouse organoids are provided in the Supplementary Tables. All material and data requests should be submitted to the corresponding author for consideration.

[10]Department of Mechanical Engineering, Boston University, Boston, MA 02215, USA

[11]Department of Molecular Biology, Massachusetts General Hospital, Boston, MA 02114, USA

[12]Division of Endocrinology, Boston Children's Hospital, Boston, MA 02115, USA

[13]Department of Clinical Immunology, Rigshospitalet, Copenhagen University Hospital, DK-2200, Copenhagen, Denmark

[14]Department of Pathology, Massachusetts General Hospital

[15]Harvard Stem Cell Institute, Cambridge, MA 02138, USA

Abstract

Background & aims: Fibrosis and tissue stiffening are hallmarks of the inflammatory bowel disease (IBD). We have hypothesized that the increased stiffness directly contributes to the dysregulation of the epithelial cell homeostasis in IBD. Here, we aim to determine the impact of tissue stiffening on the fate and function of the intestinal stem cells (ISCs).

Methods: We developed a long-term culture system consisting of 2.5-dimensional intestinal organoids grown on a hydrogel matrix with tunable stiffness. Single-cell RNA sequencing provided stiffness-regulated transcriptional signatures of the ISCs and their differentiated progeny. YAP-knockout and YAP-overexpression mice were used to manipulate YAP expression. In addition, we analyzed colon samples from murine colitis models and human IBD samples to assess the impact of stiffness on ISCs *in vivo*.

Results: We demonstrated that increasing the stiffness potently reduced the population of $LGR5^+$ ISCs and $KI\text{-}67^+$ proliferating cells. Conversely, cells expressing the stem cell marker, OLFM4, became dominant in the crypt-like compartments and pervaded the villus-like regions. Concomitantly, stiffening prompted the ISCs to preferentially differentiate toward goblet cells. Mechanistically, stiffening increased the expression of cytosolic YAP, driving the extension of $OLFM4^+$ cells into the villus-like regions, while it induced the nuclear translocation of YAP, leading to preferential differentiation of ISCs towards goblet cells. Furthermore, analysis of colon samples from murine colitis models and IBD patients demonstrated cellular and molecular remodeling reminiscent of those observed *in vitro*.

Conclusions: Collectively, our findings highlight that matrix stiffness potently regulates the stemness of ISCs and their differentiation trajectory, supporting the hypothesis that fibrosis-induced gut stiffening plays a direct role in epithelial remodeling in IBD.

Lay summary

Intestinal tissue stiffening, due to fibrosis, in inflammatory bowel disease reduces the population and stemness of the intestinal stem cells and promotes their differentiation towards goblet cells.

Graphical Abstract

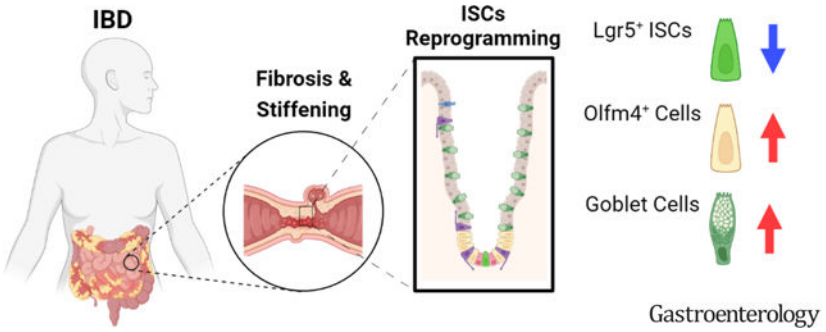

Keywords

IBD; fibrosis; stiffening; intestinal organoids; intestinal stem cells

INTRODUCTION

The intestinal stem cells (ISCs) continuously migrate on the soft basement membrane (BM) from the bottom of the crypt to the tip of the villus, differentiating into diverse types of gut epithelial cells, including goblet cells, enteroendocrine cells (EECs), tuft cells, microfold (M) cells, and enterocytes [1]. Inflammatory bowel disease (IBD), which encompasses ulcerative colitis (UC) and Crohn's disease (CD), is associated with the deterioration of gut epithelium, including loss of barrier function and alterations in the various epithelial cell populations [2–4]. Concomitantly, the excessive deposition of extracellular matrix (ECM) proteins, such as collagen types I and IV, causes the BM to stiffen [5–7]. It has been shown that tissue stiffness can regulate the differentiation of mesenchymal stem cells [8], as well as progenitor cells of the central nervous system [9], and pancreas [10].

Multiple investigations have also shown that modulation of stiffness can improve the spreading of 2D enteroids [11] and the viability of 3D gut organoids [12]. However, the influence of matrix stiffness on the stemness and differentiation of ISCs is not fully understood. Using 3D gut organoids cultured in an elegant designer matrix, Gjorevski, et al., observed that stiff matrices support the maintenance of ISC stemness [13]. This observation, however, does not align with the reduction of $LGR5^+$ ISCs observed in fibrotic, stiff gut [2, 4]. These conflicting observations may stem from the buildup of pressure inside the hydrogel due to 3D organoid growth, which generates artificial non-physiological compressive forces on the organoids [13, 14]. Yet, it is impossible to decouple the effects of matrix stiffness from the compressive forces in the 3D matrix system. Furthermore, the impact of stiffness on the ISC differentiation trajectory is yet unknown.

METHODS

Mice

Crypts were harvested from 10–14 week old mice and included the following strains: wild type C57BL/6J, *Lgr5-EGFP-IRES-CreER* [15], conditional YAP knockout, or YAP conditional overexpression. To generate the conditional YAP knockout mice, *CAG-rtTA3*

(Jackson Laboratories, 016532) mice were mated with *tetO-Cre* (Jackson Laboratory, 006234) and *Yap*$^{fl/fl}$ mice [16]. To generate the conditional YAP overexpression mice, *tetO-YAP-GFP* mice (Jackson Laboratory, 031279) expressing mutant S112A YAP were crossbred with *Villin-rtTA*M2* mice (Jackson Laboratory, 031285). 1 μg/ml doxycycline (DOX) was added to induce YAP knockout or overexpression in the organoid culture. The animals were housed and maintained on a 12-hour light/dark cycle with access to food and water ad libitum. All experimental procedures were approved by the Institutional Animal Care and Use Committee (IACUC) of the Massachusetts General Hospital and met the guidelines of National Institutes of Health (NIH).

2.5D gut organoid culture

Crypts were collected from the proximal mouse small intestine with 12 cm length or from the whole colon. Both female and male mice were used. No significant differences were detected between the organoids derived from the female and male mice. The intestine was washed with ice cold PBS (Corning, 21–040), and digested in ice-cold 10 mM EDTA (Thermo fisher, 15575020) after cutting into 5 mm~1 cm fragments for 40 minutes. After vigorously shaking the crypts were collected through a 70 μm mesh (BD Falcon). About 1500 crypts were seeded on polyacrylamide (PA) gels in 35-mm dishes. The gel surface was coated with collagen IV (details in Supplementary materials) and was flat before seeding the crypts. During the organoid growth, they deformed the surface of the soft gel, wherein the crypt region inviginated into the soft gel, forming organoids with curved indented surfaces, termed as 2.5D organoids. 1.5 ml ENR (Epidermal growth factor / Noggin / R-sponding) media/dish was added and changed every other day. 1 μM verteporfin (VP, Sigma-Aldrich, SML0534) was added to the culture to inhibit YAP nuclear translocation. After 10–11 days in culture, the cells were fixed for immunofluorescent staining, or collected using TrypLE Express (Invitrogen, 12–605-010) for flow cytometry, transfer to 3D organoid culture in Matrigel, and single cell RNA sequencing as described in Supporting Materials. Glucose uptake was tested by incubating with 2-NBDG (Cayman Chemical Company, 11046) on day 11. For measuring the level of mitochondrial superoxide, the cells were treated with 5 μM MitoSOX (M36008).

Chronic colitis mouse model induced by dextran sodium sulfate (DSS)

To induce chronic colitis, wild type 8-week-old male C57BL/6J mice were given three cycles of DSS. Each cycle included 2.5% DSS in drinking water for one week followed by pure drinking water for two weeks. Another cohort of DSS-treated animals received verteporfin (VP, 25 mg/kg/d in DMSO; Sigma-Aldrich) or vehicle (DMSO, control) via i.p. injection for two weeks immediately following the final dose of DSS or vehicle. After the three cycles of DSS, when the inflamed colon tissues were in the regenerative phase, samples were collected for stiffness measurements and immunohistochemistry (IHC) as described in Supporting Materials.

Patient samples

All human colon resection samples were provided by the Center for the Study of Inflammatory Bowel Disease at Massachusetts General Hospital under approved Institutional Review Board 2004P001067. The colon resection samples were obtained from

three male patients with UC. The strictured ileum resection samples were collected from three male patients with CD. Sample information is provided in Supplementary Table S1. The samples were processed as described in the methods of IHC and ISH in Supporting Materials.

Statistical analysis

The number of biological replicates or the number of animals is indicated in the figure legends. All experiments were performed with at least three biological replicates. For *in vitro* organoid culture, crypts were collected from each same mouse and seeded on the gels with different stiffness. For *in vivo* DSS administration, littermates were randomly assigned to groups. All confidence intervals shown on the bar chats are plotted as mean ± standard deviation of the mean. Statistical analysis for significance between two groups was performed using the two-tailed unpaired Student's *t*-test. One-way ANOVA analysis (GraphPad Prism; La Jolla, CA) assuming normal Gaussian distribution with Dunnett's test was used for the multiple group comparison. $P<0.05$ (*) was considered statistically significant.

RESULTS

2.5D Gut Organoids Cultured on Soft Hydrogel Matrix

To better understand how stiffness influences ISC fate, we cultured gut organoids on the top surface of a polyacrylamide-hydrogel matrix with tunable stiffness (Figure. 1A). While this platform faithfully recapitulates the anatomy of the gut epithelium, which is essentially a monolayer of epithelial cells residing on the top surface of the BM, it also allows for the exclusive manipulation of stiffness. A similar system was recently used to investigate the fundamental mechanisms contributing to the upward migration of crypt cells [17]. ISCs and crypts were harvested from mouse small intestine and seeded on top of the hydrogel matrix. *Lgr5-EGFP-IRES-creERT2* mice were used to track $LGR5^+$ ISCs. As the organoids grew, the soft hydrogel surface buckled (0.6 kPa, matching that of a healthy BM [5]), forming a 2.5D curved surface that mimics the invagination of *in vivo* crypts (Figure. 1B). E-cadherin staining showed an expression concentrated at the apical surface, suggesting the establishment of epithelial polarity (Figure. 1C). The crypt-like regions were densely populated by ISCs intermixed with large, optically dark UEA^+ Paneth cells (Figure. 1D). The peripheries of the crypts were surrounded by transit-amplifying (TA) cells with strong KI-67 expression, and KI-67 was also weakly expressed in $LGR5^{high}$ ISCs. The villus-like regions were primarily populated by $VILLIN^+$ enterocytes (Figure. 1D), with mature $MUC2^+$ goblet cells (Figure. 1E and Alcian Blue staining in Figure. S1A) and Chromogranin-A^+ (CHRO-A) EECs being present at significantly lower numbers (Figure. S1B), that is consistent with the composition of the *in vivo* small intestinal epithelium [18]. In addition, live-cell imaging demonstrated cells in the villus-like regions having a turnover rate of approximately 3–4 days (Figures 1F and S1C, area of villus regions quantified in Figure 1G), like that observed *in vivo*. To determine how BM stiffness influences the stemness and differentiation trajectory of ISCs, the 2.5D gut organoids were cultured on hydrogel matrices of varying stiffness.

Stiffening Reduces the Number of LGR5$^+$ ISCs and Promotes Differentiation into Mature Goblet Cells

It has been shown that healthy colon tissue has an elastic modulus around 1 kPa [5], which is increased by at least one order of magnitude in fibrotic IBD colon [6]. Thus, to determine the effects of stiffness on ISC fate, we cultured crypts on hydrogels with three stiffness values, ranging from 0.6 kPa to 9.6 kPa. Matrix stiffening potently decreased the crypt surface area and reduced the number of LGR5-EGFP$^+$ ISCs (Figure. 2A and 10-day live-cell image in Figure. S1D). The depth of the crypt invagination was also decreased (Figure. S1E). The stiffness-induced reduction of crypt surface area has also been reported in a recent study [17]. Flow cytometry analysis (Method) further confirmed the reduction of LGR5-EGFP^{high} cells and LGR5-EGFP^{low} cells, which have been identified as ISCs and progenitor cells, respectively [15, 19], on the stiff matrix (Figure. 2B). To further assess how stiffness impacts ISC stemness, after 11 days of culture, the cells were detached from their underlying hydrogel and transferred to grow 3D organoids within Matrigel® (Method). The 3D organoids generated from cells that were preconditioned on soft and medium matrices budded to form crypt-like regions with LGR5-EGFP$^+$ ISCs. Conversely, cells preconditioned on the stiff matrix generated cyst-like organoids with a significantly smaller number of buddings and negligible LGR5 expression (Figures. 2C and S1F). The cyst-like organoids also displayed a substantially pronounced population of VILLIN$^+$ differentiated cells (Figure. S1G). Thus, the loss of ISC stemness caused by stiffening was persistent and did not recover after transferring into Matrigel. This observation indicates that the impacts of gut stiffening are memorized by ISCs and can persist even during the remission period of IBD.

Compared to the well-studied role of LGR5 in activating WNT signaling pathway, the functions of another stem cell marker, Olfactomedin-4 (OLFM4) are not yet fully understood. It is demonstrated that OLFM4 is a target of the NOTCH signaling [20] which can also negatively regulate WNT/β-catenin activation [21]. Here, we found that the expression and distribution of OLFM4, was also strongly influenced by matrix stiffness (Figure. 2A). On the medium and stiff substrates, OLFM4$^+$ cells can replace the LGR5$^+$ ISCs and became dominant in the crypt region (Figure. S1H) and extended into villus-like regions (Figure. 2A).

Live-cell imaging on the soft matrix depicts how the LGR5-EGFP$^+$ ISCs divide and differentiate into large, optically dark Paneth cells (Figure. S1I and Movie S1). The generation of Paneth cells is thought to be critical for long-term maintenance of the ISC niche and stemness [22]. Intriguingly, the long-term live cell imaging demonstrated that, on the stiff matrix, the LGR5$^-$ cells in the villus-like regions directly differentiated into Paneth cells around which new crypt-like regions formed (Figure. 2D and Movie S2). In the brightfield images, the crypt regions were easily distinguishable by the presence of the large and dark Paneth cells (Figure. S1J). Moreover, other cells in the crypt regions were much denser and smaller than the cells in the villus regions. The incidence of these new crypt formations was approximately threefold higher on stiff matrix compared to soft matrix (Figure. S1K). Considering the absence of LGR5 expression in the villus-like regions, this result suggests OLFM4$^+$ cells may give rise to the formation of the new crypts.

Matrix stiffness also profoundly impacted the differentiation trajectory of the ISCs. Increasing the stiffness significantly reduced the populations of KI-67^{+} proliferating cells, the Lysozyme (LYZ)$^{+}$ Paneth cells, the enterocytes (marked by VILLIN and ALPI), and the CHRO-A^{+} EECs (Figures. 2E and S2A). In contrast, the marker of secretory progenitor cells, DLL1, and the goblet cell marker, MUC2 were increased (Figures. 2E and S2A). The side views consistently showed that increasing stiffness decreased the expression of KI-67 and LGR5 in the invaginated crypt regions and the VILLIN expression and promoted the expression of MUC2 (Figure. S2B). Examination of the MUC2 staining images demonstrated the presence of two distinct cell populations on the stiff substrate: those with strong MUC2 expression (i.e., MUC2^{hi}) and a population with weak MUC2 expression (i.e., MUC2^{low}, Figure. 2E). Intriguingly, co-staining for Alcian Blue (AB), which marks mature goblet cells, and MUC2 demonstrated that only the MUC2^{hi} cells were AB-positive, suggesting that the MUC2^{hi} cells were mature goblet cells (Figure. S2C).

Consistent with this observation, there were approximately a 6-fold increase in the populations of both MUC2^{hi} and AB+ cells on the stiff substrate (Figure. 2E and S2A). The MUC2^{low} cells simultaneously expressed ALPI (Figure. S2D), and stem cell marker, OLFM4 (Figure. S2E). We referred these cells as immature enterocyte-goblet cell (IEGC), where ‘immature’ refers to the co-expression of multiple cell type markers. Flow cytometry analysis (Method) confirmed the reduction of KI-67^{+} proliferating cells (Figure. 2F) and Paneth cells (CD24^{high}, C-KIT^{+} and SSC^{high}, Figure. 2G) on stiff matrix.

Notably, a similar self-organizing, crypt-villus structure and stiffness-dependent phenotype are also observed when flow cytometry-sorted single LGR5^{+} cells were cultured, wherein stiffening decreased the populations of LGR5^{+} and VILLIN^{+} cells, and increased MUC2^{+} cells (Figures. S2F–S2I). We also performed analogous analyses on the organoids derived from colon crypts. Increasing substrate stiffness diminished the population of LGR5^{+} ISCs and KI-67^{+} proliferating cells (Figure. S3A–S3C). Furthermore, the expression of the enterocyte marker, ALPI, was reduced, whereas MUC2 expression was increased on the stiff substrate (Figure. S3D and S3E). Thus, the influence of stiffness on colon ISCs is similar to that we observed in small intestinal ISCs.

The schematic in Figure. 2H summarizes the influence of stiffening on the fate of ISCs: in the crypt-like regions, stiffening led to a loss of LGR5^{high} ISCs and reduced the population of LGR5^{low}, KI-67^{+} TA progenitor cells. In the villus-like regions, stiffening led to the replacement of the VILLIN^{+} mature enterocytes by MUC2^{+}, VILLIN^{+}, and OLFM4^{+} IEGCs and mature goblet cells.

Stiffness Differentially Regulates YAP in Crypts and Villus Regions

We asked whether the mechano-transducer, YAP, plays a role in the regulation of ISC fate by stiffness. On the soft matrix, YAP expression was exclusively observed in the crypt region, and increasing the stiffness led to a significant increase in YAP expression and nuclear translocation across both crypt and villus-like regions (Figures. 3A and 3B). Consistently, stiff substrate also promoted the YAP nuclear translocation of colon organoids (Figure. S3F and S3G). To better distinguish the expression patterns of nuclear YAP (nuc-YAP) and cytoplasmic YAP (cyto-YAP), and since YAP phosphorylation inhibits its nuclear

translocation [23], we performed immunofluorescence of non-phosphorylated nuc-YAP and Ser-127 phosphorylated cyto-YAP, respectively. We observed that nuc-YAP expression was increased across both the crypt- and villus-like regions on stiff matrix (Figure. 3C). In contrast, cyto-YAP exhibited a strong region-dependent expression pattern, wherein it was decreased by stiffening in the crypt-like regions but increased in the villus-like regions (Figure. 3D).

Stiffness-dependent Expressions of Nuc-YAP and Cyto-YAP Play Divergent Roles in Determining the Fate of ISCs

To assess how the stiffness-dependent YAP expression and sequestration impact ISC fate, we manipulated YAP via transgenic mouse models with doxycycline (DOX)-inducible conditional YAP knockout (cKO: *CAG-rtTA3*; *tetO-Cre*; $Yap^{flox/flox}$) or YAP overexpression (cOE: *villin-rtTA*M2*; *tetO-YAP-GFP*) (Method). Then, crypts were harvested from naïve animals and the transgene was induced *in vitro*. Also, YAP inhibitor, verteporfin (VP), was used to suppress YAP nuclear translocation [24]. We observed that $LGR5^+$ ISCs were YAP negative, and YAP expression was inversely correlated with LGR5 expression (Figure. 4A, as quantified in Figure 4D). YAP OE on the soft substrates led to the disappearance of the crypt-like regions (Figure. 4B), causing a shift towards the stiff matrix-like phenotypes. Conversely, VP administration on the stiff matrix led to the formation of large crypt-like regions and restored LGR5 expression (Figure. 4C, as quantified in Figure 4D), bestowing the soft matrix-like phenotypes. These observations demonstrated that YAP activation inhibits LGR5 expression.

The goblet cell marker, MUC2, was strongly correlated with YAP nuclearization (Figure. 4E, as quantified in Figure. 4H). Comparing the phenotypes between the YAP OE on the soft substrate and the VP administration on the stiff substrate demonstrates that increasing nuc-YAP expression by YAP OE promoted MUC2 (Figures. 4F and S4A), whereas decreasing nuc-YAP by VP suppressed MUC2 (Figure. 4G, as quantified in Figure. 4H).

On the other hand, OLFM4 expression in the villus region exhibited strong correlation with cytoplasmic YAP, wherein induction of OLFM4 on medium stiffness was associated with the appearance of cytoplasmic YAP expression (Figure. 4I). Consistently, compared with the medium substrate, the reduction in cytoplasmic YAP on stiff substrate caused by the enhanced YAP nuclearization was associated with the reduction in OLFM4 expression (Figure. 4I, as quantified in Figure. 4L). Meanwhile, augmentation of cytoplasmic YAP by both YAP cOE (Figures. 4J and S4B) and VP administration (Figure. 4K) persistently increased the expression of OLFM4, confirming that cyto-YAP positively regulates OLFM4 (as quantified in Figure. 4L).

YAP KO on both soft and stiff substrates led to the loss of villus-like regions (Figure. S4C). The leftover crypt-like regions were enriched with Paneth cells and were negative for nuc-YAP and cyto-YAP, as well as MUC2, OLFM4, and VILLIN (Figures. S4D and S4E as quantified in Figure. S4F). These data demonstrated the indispensability of YAP to the differentiation of ISCs and the generation of villi.

Here, the combination of mechanical, genetic, and pharmacological manipulation of YAP expression and sequestration discriminate the functional roles of nuc-YAP and cyto-YAP in the regulation of ISC stemness and differentiation, i.e., YAP is indispensable for ISC differentiation and villus generation; and stiffening-induced YAP nuclearization suppresses the population of $LGR5^+$ ISCs and drives the differentiation into goblet cells, while cyto-YAP drives the differentiation towards $OLFM4^+$ cells.

Stiffness-Regulated Transcriptional Signatures of ISCs and Their Differentiated Progeny

To provide a comprehensive map of how stiffness impacts ISCs and their differentiated progeny at the transcriptional level, we performed single-cell RNA sequencing (scRNAseq) analysis. The single-cell expression profiles of our 2.5D gut organoids were clustered into thirteen cell groups (Figure. 5A and Supplementary Table 1). Thirty Principal components were selected for the dimensional reduction based on their statistical significance ($P<0.05$). Cluster annotation using known epithelial marker genes [25] revealed that all the different types of progenitors and differentiated gut epithelial cells are present in the *in vitro* system (Figures. 5A, 5B, and S5). The trajectory inference using Partition-based graph abstraction (PAGA) [26] demonstrated a trajectory from stem cells and TA cells to the progenitor cells to the differentiated cell populations (Figure. S6). Clustering was consistent across the biological triplicated samples for both soft and stiff conditions (Figure. S7A and Method). IEGCs simultaneously expressed mild levels of marker genes for stemness, enterocytes, and goblet cells (Figures. 5B, S2D and S2E). scProportionTest analysis (Method) also confirmed the effects of stiffening on the ISC differentiation trajectory, including a 25% and 42% reduction in ISCs and tuft cells, respectively (Figure. 5C). Goblet cells, M cells and IEGCs were increased by 28%, 24% and 25%, respectively. Differential expression analysis (Supplementary Table 2) and immunofluorescence imaging showed extensive and widespread expression of another goblet cell marker, Trefoil factor 3 (Tff3) across the whole villus region on the stiff substrate (Figure. 5D).

We next assessed the expression levels of the known YAP-upregulated and downregulated genes previously curated by Gregorieff, et al. [27]. The top 18 YAP-downregulated genes showed consistently greater expression in both enterocytes and enterocyte progenitors, whereas the top 17 YAP-upregulated genes showed greater enrichment in goblet cells, IEGCs, and M cells (Figure. 5E and S7B). Furthermore, the gene expressions of *Id2*, *Birc5*, and *Areg*, which are downstream of nuc-YAP [28], were significantly increased on stiff matrix (Figure. S7C). Pathway enrichment analysis (PEA) also revealed an upregulation of mechanotransduction signaling pathways, including actin cytoskeleton, focal adhesion, and tight junctions, potentially contributing to YAP activation (Figure. S7D). These results further corroborate that matrix stiffening activates YAP, which in turn mediates the differentiation of ISCs towards goblet cells, as opposed to enterocytes.

Stiffening suppressed the gene expression of *Lgr5* and *Sox4*, a WNT/β-catenin agonist [29], in ISCs (Figure. S7E), consistent with the loss of stemness on stiff matrix. Furthermore, *Hes1*, a Notch pathway target gene [30], was also downregulated on stiff matrix (Figure. S7E). HES1 inhibition is known to promote goblet cell differentiation at the expense of enterocytes [31], which is also in accordance with stiffening-enhanced goblet cell differentiation. In

addition, the PROGENy activity scores (Methods) [32] across all the cells demonstrated that the WNT, TGFb, and MAPK pathways were significantly activated on the soft substrate. Conversely, TRAIL pathways were significantly activated on the stiff substrate (Figure. S8A). The PROGENy activity scores of each cell population showed that ISCs and enterocyte progenitor cells contributed to the different WNT activity on the soft vs. stiff substrate; enterocyte progenitor cells and Microfold cells to the different TGFb activity; ISCs, enterocyte progenitor cells and goblet cells to the different activities of TRAIL and MAPK pathways (Figure. S8B).

The scRNAseq analysis further suggested that stiffening strongly influences the metabolic activity and demand of cells, the hallmark of which was increased carbon metabolism (from PEA, Figures. 5F and S7F). In particular, the glycolytic pathway, tricarboxylic acid (TCA) cycle, and oxidative phosphorylation pathway were all upregulated on stiff substrate (Figure. 5F and the corresponding genes in Supplementary Table 3), suggesting augmented glucose utilization and catabolism. The direct assessment of glucose uptake, mitochondrial reactive oxygen species (MitoSOX™, direct byproducts of oxidative phosphorylation) (Figure. 5G) and expression of the glucose transporter 2, GLUT2 (Figure. 5H) corroborated with the high demand of glucose on stiff matrix. Intriguingly, inhibiting glucose uptake on stiff matrix via the pan-class I GLUT inhibitor, Glutor, increased crypt size and decreased MUC2 expression, resulting in a shift towards soft matrix-like phenotypes (Figure. 5I). These results demonstrate that matrix stiffening potently augments glucose metabolism in ISCs and their progeny, and that the resultant metabolic rewiring plays a critical role in mediating the effects of stiffness on ISC fate.

Colon Stiffening Triggers ISC Remodeling in Murine Model of Colitis

To verify our *in vitro* observations on the role of stiffness in determining ISC fate, we utilized a mouse model of chronic colitis, in which the animals were administered three weeks of dextran sodium sulfate (DSS, or water as control), each of which was interspersed by two weeks of recovery [33]. Furthermore, another cohort of DSS-treated animals received VP (or DMSO as control) throughout the final two weeks of recovery (Method), during which the epithelium was regenerated from inflammation-induced damage (Figure 6A). We confirmed that VP or DMSO administration in the no-DSS control groups did not induce detectable changes. In the colitis model, the colon stiffened and thickened (Figure 6B). Similar to our *in vitro* observations, the stiffened colitis colon was associated with increased nuc-YAP expression, and VP administration in the DSS-induced colitis mice suppressed nuc-YAP expression and increased cyto-YAP (Figure. 6C). The YAP expression pattern was consistent across the entire colon epithelium (Figure. S4G). Consistently, LGR5 expression decreased in the colitis colons, and was recovered after VP administration Consistently, LGR5 expression decreased in the colitis colons, and was recovered after VP administration (Figure. 6D). Also, the extensive presence of goblet cells exhibited in the colitis colon brush borders and was inhibited after VP administration (Figure. 6E). Consistent with our *in vitro* observations, VP administration in colitis mice potently recovered the LGR5 expression and suppressed both nuc-YAP expression and goblet cell differentiation, reversing the effects of colon stiffening. In addition, VP administration mitigated the body weight loss and colon thickening of DSS-induced colitis mice (Figure. S4H).

Stiffness-Induced ISC remodeling in Human IBD Patients

To determine the extent to which the stiffening-induced remodeling of our gut organoids and murine gut epithelium resembles that of human IBD patients, we analyzed scRNAseq data generated from colon resection samples of IBD patients and healthy individuals [34]. The human single cell profiles were clustered into ten epithelial cell subsets which were annotated using known marker genes (Figures. S9A and S9B). IBD was associated with a decrease in patients' ISC and enterocyte populations, and an increase in goblet cells (Figures. 7A and S9C with and without accounting for sample size, respectively), which are consistent with the phenotypes of substrate stiffening observed *in vitro*. Pathway enrichment analysis demonstrated strong activation of the pathways involved in ECM biosynthesis (including *COLLAGEN I* and *IV*) in IBD, which is indicative of increased fibrosis and stiffening (Figure. 7A). Concomitantly, *WNT* signaling was suppressed in the ISC population of IBD patients (Figure. 7A and S9D). In addition, there was potent activation of the mechanosignaling pathway, including *INTEGRIN*, *YAP*, and *TEAD* (the primary transcription factors for YAP), in both the ISCs and the goblet cells of patients with UC, but not in the enterocytes (Figure. S9E). In agreement with this observation, the established YAP-upregulated genes [27] were enriched in both ISC and goblet cell populations of IBD colon (Figure. 7A). The scRNAseq analysis of the human IBD and healthy samples identified similar key features compared to those observed from the *in vitro* organoids. Most notably, in IBD patients the population of ISCs decreased and goblet cells increased. In addition, YAP signaling pathway is upregulated and Wnt signaling pathway is suppressed in ISCs.

Histomorphometric analysis of human colon tissues demonstrated thickening of the BM and lamina propria, and the disappearance of enterocyte brush borders (Figure. 7B), and excessive collagen deposition and fibrosis (Figures. 7C and 7D) in IBD. The number of KI-67$^+$ proliferating cells and LGR5$^+$ ISCs was significantly decreased in IBD samples (Figure. 7E). Conversely, OLFM4 expression was increased and extended into the apical surface (Figure. 7F), consistent with previous reports [35]. Notably, in extremely fibrotic and strictured ileum samples, the invaginated ISC niche-crypts nearly disappear and only pieces of the villi remain, resembling the stiffness-reduced size of the crypt and loss of ISCs (Figure. 7G). Meanwhile, numerous ectopic crypts have formed, resembling the stiffness-induced new crypt formation, which, despite negligible LGR5 expression, exhibited strong OLFM4 expression (Figure. 7G). Like our *in vitro* observations, MUC2$^+$ goblet cells were overwhelmingly present in IBD colon compared to healthy tissues (Figure. 7H). Notably, there was strong YAP expression and nuclear localization in the IBD samples (Figure. 7I). The scRNAseq and histology data from human IBD patients strongly complemented our *in vitro* observations, demonstrating that gut stiffening is associated with strong YAP upregulation, loss of ISCs, extension of OLFM4 expression, and enhanced differentiation towards goblet cells. Together, these results suggest that stiffness plays a direct and critical role in epithelial remodeling in IBD.

Therefore, on the basis of our complementary *in vitro* and *in vivo* observations, we have demonstrated that stiffness regulates ISC fate via YAP, wherein the stiffness-induced loss of

LGR5$^+$ ISCs and the differentiation toward MUC2$^+$ goblet cells is mediated by nuc-YAP. On the other hand, cyto-YAP drives the differentiation toward OLFM4$^+$ cells (Figure. 7J).

DISCUSSION

Previous studies with the purpose of designing *in vitro* 3D matrices for 3D organoid culture showed that the stiffer matrix promoted ISC expansion and the softer matrices enhanced crypt budding and ISC differentiation [13]. However, these phenotypes are not consistent with the reduction of ISCs in the fibrotic stiff intestine in IBD [2, 4]. This could be due to challenges associated with tuning stiffness in 3D hydrogel matrices, which causes secondary effects such as increased pressure. Furthermore, considering that the *in vivo* intestinal epithelium has a monolayer structure with an open lumen, our systems represent a higher-physiological relevance, particularly in the context of studying cell-matrix biophysical interactions. Moreover, the influence of stiffness on the differentiation trajectory of ISCs is still not clear. Using our 2.5D organoids, we discovered that matrix stiffening potently reduced the LGR5$^+$ ISC population. Additionally, the increased stiffness led to the expansion of OLFM4 from crypts to villus regions and promoted the differentiation of ISCs towards goblet cells. All these phenotypes were similarly observed in stiff colon samples from the murine colitis model and human IBD patients.

YAP is a critical regulator of intestinal epithelial regeneration during inflammation [4] and tumorigenesis [27, 36]. YAP activation can suppress WNT pathway and diminish LGR5$^+$ ISCs [4, 36], and can also promote the differentiation into Paneth cells [37] and goblet cells [38]. On the other hand, YAP activation induces a regenerative program via activating fetal marker genes (e.g., expressing *Sca1* and *Anxa1*) [4] and EGFR signaling [27]. We further demonstrated that YAP, as a downstream of tissue stiffness, plays a critical role in the intestinal epithelial regeneration during IBD. Most notably, we comprehensively elucidated the divergent roles of cyto-YAP and nuc-YAP in determining the ISC differentiation trajectory. Matrix stiffening-induced cyto-YAP expression drove the extension of OLFM4$^+$ cells into villus-like regions, whereas nuc-YAP expression led to a loss of LGR5$^+$ ISCs and increased differentiation toward goblet cells. The results of the scRNAseq analysis provided the stiffness-regulated transcriptional signatures of ISCs and their differentiated progeny, further corroborating the stiffness-dependent regulation of the ISC stemness and differentiation trajectory via YAP.

The metabolic pathway enrichment analysis as well as the direct assessment of glucose uptake and mitochondrial reactive oxygen species demonstrated that matrix stiffening augments ISC glucose demand and metabolism. Moreover, inhibiting glucose uptake on stiff matrix led to a shift toward soft matrix-like phenotype. These results are in-line with emerging evidence of the link between mechanical stimuli and energy metabolism [39]. Moreover, the activation of YAP could serve as a central core by sensing the mechanical stimuli to promote glucose metabolism [40]. In addition, it has been observed that intestinal tissues display elevated glucose metabolism in IBD [41]. Thus, the intestinal stiffening during IBD could mediate the fate of ISCs via YAP-induced metabolic rewiring. Therefore, exploiting the metabolic vulnerability of the mechano-stimulated ISCs could potentially offer a novel therapeutic strategy for IBD.

During the growth of the organoids, the cells in the crypt regions buckle the surface of the soft substrate, creating a curved invaginations that mimics the *in vivo* crypt morphology. It is notable that the radius of the curvature in the crypt regions, even on the soft substrate, exceeds 250 μm. In comparison, the diameter of an ISC is in the order of 10 μm. Considering that a cell can sense a curvature when the curvature radius is in the same order of the cell size [42], we do not anticipate considerable influence from the curvature in our system. Further investigations are warranted to determine how deeper curvatures influence the mechanobiology of ISCs and their communication with the Paneth cells which constitute their niche.

The potent impact of gut stiffening on OLFM4 expression and expansion may also have important implications in the context of IBD and colitis-associated colorectal adenocarcinoma (CAC). More specifically, while sporadic colorectal carcinoma (CRC) is shown to be LGR5 positive [43], most colitis-associated CACs lack LGR5 expression [44]. The mechanisms through which the two ISC markers – LGR5 and OLFM4, differently regulate CAC development remain to be determined. Here, in both the *in vitro* model and in the stiff human IBD colon, we observed that stiffening leads to an extension of OLFM4 into villus regions. This phenotype is reminiscent of our *in vitro* observations in which, on the stiff substrate, the $OLFM4^{+}$, $LGR5^{-}$ cells in the villus regions continuously gave rise to new crypts. This finding suggests that the $OLFM4^{+}$ cells in stiff colon are capable of generating new crypts, which could potentially lead to the development of CAC. Therefore, the signaling pathways involved in stiffening-induced OLFM4 extension might be potential clinical targets for colitis-associated CAC.

Supplementary Material

Refer to Web version on PubMed Central for supplementary material.

Acknowledgments

This work was supported by funding from National Institutes of Health (R01DK123219 and K01DK103947 to N.S., and R01HL148152 and U01CA202123 to J.J.F.), ECOR/MGH (2019A002949 to N.S.), and Polsky family fund (to N.S.). We thank Dr. Ramnik J. Xavier, the Director of the Center for the Study of Inflammatory Bowel Disease at Massachusetts General Hospital (National Institutes of Health, P30DK043351) for his constructive comments, providing human samples and sharing the human scRNAseq data. We thank Maris A. Handley and Jacqueline Choi from the HSCI-CRM Flow Cytometry Core and iHisto Inc. for their support. We also thank Ann S. Adams for editorial advice.

REFERENCE

1. Bloemendaal AL, Buchs NC, George BD, et al. Intestinal stem cells and intestinal homeostasis in health and in inflammation: a review. Surgery 2016;159:1237–1248. [PubMed: 26936524]
2. Schmitt M, Schewe M, Sacchetti A, et al. Paneth cells respond to inflammation and contribute to tissue regeneration by acquiring stem-like features through SCF/c-Kit signaling. Cell reports 2018;24:2312–2328. e7. [PubMed: 30157426]
3. Wang Y, Chiang I-L, Ohara TE, et al. Long-term culture captures injury-repair cycles of colonic stem cells. Cell 2019;179:1144–1159. e15. [PubMed: 31708126]
4. Yui S, Azzolin L, Maimets M, et al. YAP/TAZ-dependent reprogramming of colonic epithelium links ECM remodeling to tissue regeneration. Cell Stem Cell 2018;22:35–49. e7. [PubMed: 29249464]

5. Stewart DC, Berrie D, Li J, et al. Quantitative assessment of intestinal stiffness and associations with fibrosis in human inflammatory bowel disease. PloS one 2018;13.
6. Johnson LA, Rodansky ES, Sauder KL, et al. . Matrix stiffness corresponding to strictured bowel induces a fibrogenic response in human colonic fibroblasts. Inflammatory bowel diseases 2013;19:891–903. [PubMed: 23502354]
7. He S, Azar DA, Esfahani FN, et al. Mechanoscopy: A Novel Device and Procedure for in vivo Detection of Chronic Colitis in Mice. Inflammatory Bowel Diseases 2022;28:1143–1150. [PubMed: 35325126]
8. Engler AJ, Sen S, Sweeney HL, et al. Matrix elasticity directs stem cell Lineage specification. Cell 2006;126:677–689. [PubMed: 16923388]
9. Segel M, Neumann B, Hill MF, et al. Niche stiffness underlies the ageing of central nervous system progenitor cells. Nature 2019;573:130–134. [PubMed: 31413369]
10. Mamidi A, Prawiro C, Seymour PA, et al. Mechanosignalling via integrins directs fate decisions of pancreatic progenitors. Nature 2018;564:114–118. [PubMed: 30487608]
11. Altay G, Larrañaga E, Tosi S, et al. Self-organized intestinal epithelial monolayers in crypt and villus-like domains show effective barrier function. Scientific reports 2019;9:1–14. [PubMed: 30626917]
12. Cruz-Acuña R, Quirós M, Farkas AE, et al. Synthetic hydrogels for human intestinal organoid generation and colonic wound repair. Nature cell biology 2017;19:1326–1335. [PubMed: 29058719]
13. Gjorevski N, Sachs N, Manfrin A, et al. Designer matrices for intestinal stem cell and organoid culture. Nature 2016;539:560–564. [PubMed: 27851739]
14. Pérez-González C, Ceada G, Matejčić M, et al. Digesting the mechanobiology of the intestinal epithelium. Current opinion in genetics & development 2022;72:82–90. [PubMed: 34902705]
15. Barker N, Van Es JH, Kuipers J, et al. Identification of stem cells in small intestine and colon by marker gene Lgr5. Nature 2007;449:1003–1007. [PubMed: 17934449]
16. Schlegelmilch K, Mohseni M, Kirak O, et al. Yap1 acts downstream of α-catenin to control epidermal proliferation. Cell 2011;144:782–795. [PubMed: 21376238]
17. Pérez-González C, Ceada G, Greco F, et al. . Mechanical compartmentalization of the intestinal organoid enables crypt folding and collective cell migration. Nature Cell Biology 2021:1–13.
18. Karam SM. Lineage commitment and maturation of epithelial cells in the gut. Frontiers in Bioscience-Landmark 1999;4:286–298.
19. Snippert HJ, Van Der Flier LG, Sato T, et al. Intestinal crypt homeostasis results from neutral competition between symmetrically dividing Lgr5 stem cells. Cell 2010;143:134–144. [PubMed: 20887898]
20. VanDussen KL, Carulli AJ, Keeley TM, et al. Notch signaling modulates proliferation and differentiation of intestinal crypt base columnar stem cells. Development 2012;139:488–497. [PubMed: 22190634]
21. Liu W, Li H, Hong S, et al. Olfactomedin 4 deletion induces colon adenocarcinoma in ApcMin/+ mice. Oncogene 2016;35:5237–5247. [PubMed: 26973250]
22. Sato T, Van Es JH, Snippert HJ, et al. Paneth cells constitute the niche for Lgr5 stem cells in intestinal crypts. Nature 2011;469:415–418. [PubMed: 21113151]
23. Dobrokhotov O, Samsonov M, Sokabe M, et al. Mechanoregulation and pathology of YAP/TAZ via Hippo and non-Hippo mechanisms. Clinical and translational medicine 2018;7:1–14. [PubMed: 29318404]
24. Wang C, Zhu X, Feng W, et al. Verteporfin inhibits YAP function through up-regulating 14–3-3σ sequestering YAP in the cytoplasm. American journal of cancer research 2016;6:27. [PubMed: 27073720]
25. Haber AL, Biton M, Rogel N, et al. A single-cell survey of the small intestinal epithelium. Nature 2017;551:333–339. [PubMed: 29144463]
26. Wolf FA, Hamey FK, Plass M, et al. PAGA: graph abstraction reconciles clustering with trajectory inference through a topology preserving map of single cells. Genome biology 2019;20:1–9. [PubMed: 30606230]

27. Gregorieff A, Liu Y, Inanlou MR, et al. Yap-dependent reprogramming of Lgr5+ stem cells drives intestinal regeneration and cancer. Nature 2015;526:715–718. [PubMed: 26503053]
28. Hong W, Guan K-L. The YAP and TAZ transcription co-activators: key downstream effectors of the mammalian Hippo pathway, In Seminars in cell & developmental biology, Elsevier, 2012.
29. Sinner D, Kordich JJ, Spence JR, et al. Sox17 and Sox4 differentially regulate β-catenin/T-cell factor activity and proliferation of colon carcinoma cells. Molecular and cellular biology 2007;27:7802–7815. [PubMed: 17875931]
30. Ohtsuka T, Ishibashi M, Gradwohl G, et al. Hes1 and Hes5 as notch effectors in mammalian neuronal differentiation. The EMBO journal 1999;18:2196–2207. [PubMed: 10205173]
31. Jensen J, Pedersen EE, Galante P, et al. Control of endodermal endocrine development by Hes-1. Nature genetics 2000;24:36–44. [PubMed: 10615124]
32. Schubert M, Klinger B, Klünemann M, et al. Perturbation-response genes reveal signaling footprints in cancer gene expression. Nature communications 2018;9:1–11.
33. Wirtz S, Popp V, Kindermann M, et al. . Chemically induced mouse models of acute and chronic intestinal inflammation. Nature protocols 2017;12:1295. [PubMed: 28569761]
34. Smillie CS, Biton M, Ordovas-Montanes J, et al. Intra-and inter-cellular rewiring of the human colon during ulcerative colitis. Cell 2019;178:714–730. e22. [PubMed: 31348891]
35. Gersemann M, Becker S, Nuding S, et al. Olfactomedin-4 is a glycoprotein secreted into mucus in active IBD. Journal of Crohn's and Colitis 2012;6:425–434.
36. Barry ER, Morikawa T, Butler BL, et al. Restriction of intestinal stem cell expansion and the regenerative response by YAP. Nature 2013;493:106–110. [PubMed: 23178811]
37. Serra D, Mayr U, Boni A, et al. Self-organization and symmetry breaking in intestinal organoid development. Nature 2019;569:66–72. [PubMed: 31019299]
38. Imajo M, Ebisuya M, Nishida E. Dual role of YAP and TAZ in renewal of the intestinal epithelium. Nature cell biology 2015;17:7–19. [PubMed: 25531778]
39. Evers TM, Holt LJ, Alberti S, et al. Reciprocal regulation of cellular mechanics and metabolism. Nature metabolism 2021;3:456–468.
40. Koo JH, Guan K-L. Interplay between YAP/TAZ and Metabolism. Cell metabolism 2018;28:196–206. [PubMed: 30089241]
41. Bhattaru A, Borja A, Zhang V, et al. FDG-PET/CT as the superior imaging modality for inflammatory bowel disease. The Journal of Nuclear Medicine 2020;61:1159.
42. Assoian RK, Bade ND, Cameron CV, et al. Cellular sensing of micron-scale curvature: a frontier in understanding the microenvironment. Open biology 2019;9:190155.
43. Hirsch D, Barker N, McNeil N, et al. . LGR5 positivity defines stem-like cells in colorectal cancer. Carcinogenesis 2014;35:849–858. [PubMed: 24282287]
44. Iwaya M, Ota H, Nakajima T, et al. Most colitis associated carcinomas lack expression of LGR5: a preliminary study with implications for unique pathways of carcinogenesis compared to sporadic colorectal carcinoma. BMC cancer 2021;21:1–9. [PubMed: 33397301]

WHAT YOU NEED TO KNOW

BACKGROUND

Fibrosis and tissue stiffening are hallmarks of inflammatory bowel disease (IBD). Yet, it is unclear how the tissue stiffening impacts the fate of intestinal stem cells (ISCs).

NEW FINDINGS

Stiffening reduces the population of $Lgr5^{hi}$ ISCs and $Ki67^{+}$ progenitor cells, extends Olfm4 expression from the crypt-like compartments into the villus-like regions, and promotes ISCs to preferentially differentiate to goblet cells.

LIMITATIONS

Directly preventing or inhibiting intestinal fibrosis and stiffening in colitis mice is not included due to lack of reliable strategies. The colitis mouse model was performed using male mice.

CLINICAL RESEARCH RELEVANCE

We elucidated how intestinal stiffening reprogram the ISC fate during IBD, leading to the intestinal epithelial deterioration. In addition, the Olfm4 expression extended on the stiff substrate may induce colitis-associated colorectal adenocarcinoma. These results identify tissue stiffening and mechanosignaling pathways as potential targets for IBD.

BASIC RESEARCH RELEVANCE

We developed a novel platform of culturing 2.5D intestinal organoids that closely mimics the native tissue. Using this model, we identified the influence of stiffness on ISCs and the mediating role of YAP signaling. These results, and the 2.5D gut organoid platform, would inspire mechanistic investigations into the crosstalk between mechanotransduction, metabolism, and other signaling pathways that regulate ISC function.

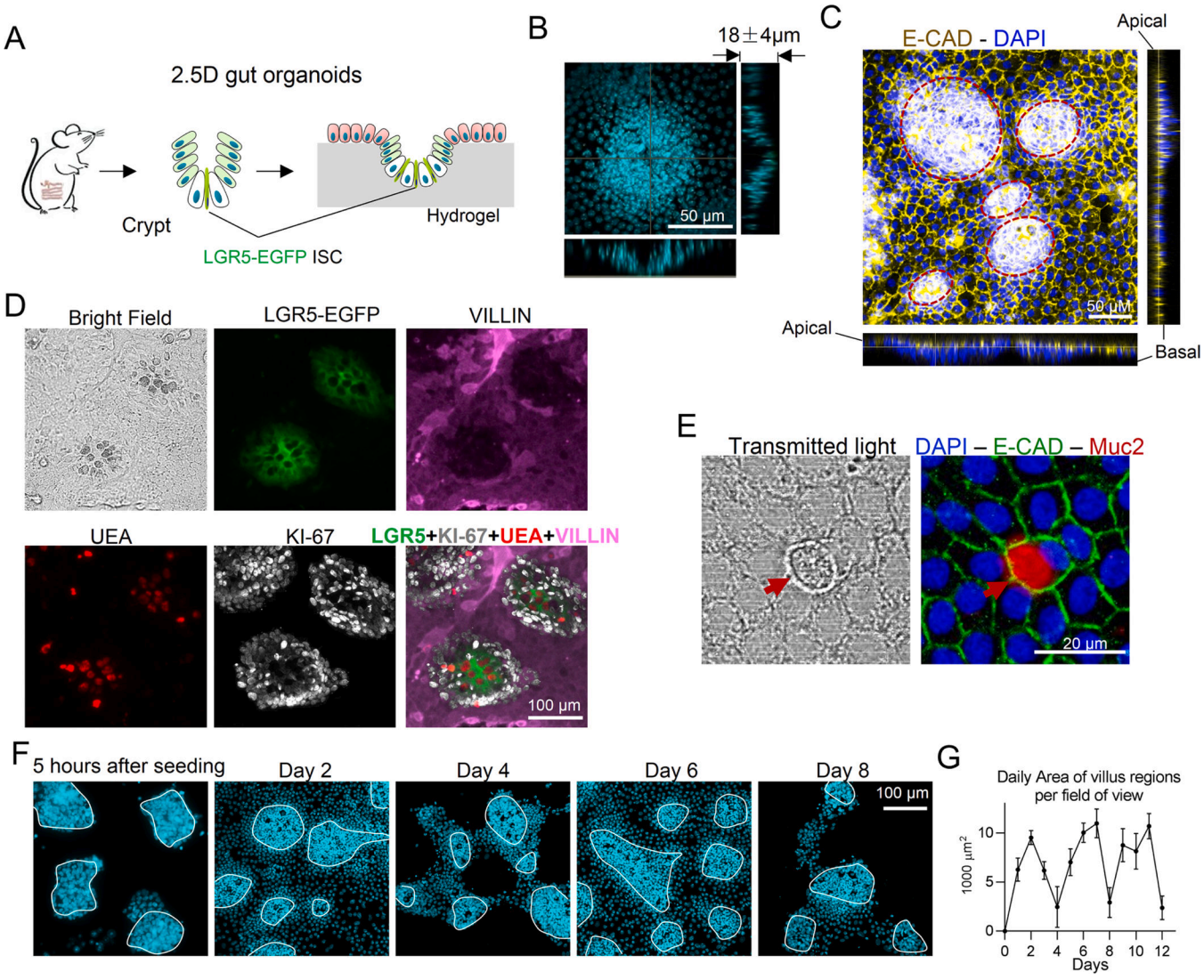

Figure 1. 2.5D gut organoids cultured on soft hydrogel matrices.

(A) Illustration of the experimental system. (B) Orthogonal projection of DAPI staining showing the invagination of crypt-like region with dense nuclei. Scale bar, 50 μm. (C) Orthogonal projection of E-cadherin staining showing a concentrated expression at the apical surfaces (n=3). The red dashed lines indicate crypt regions. Scale bar, 50 μm. (D) LGR5-EGFP$^+$ ISCs were intermixed with the optically dark and UEA$^+$ Paneth cells, which were surrounded by KI-67$^+$ TA cells in the crypt-like regions. The villus-like regions were populated by villin$^+$ differentiated cells (n=3). Scale bar, 100 μm. (E) The confocal transmitted light image showed distinguishable morphology of MUC2$^+$ goblet cells (n=3). Scale bar, 20 μm. (F) DAPI staining showed that the villus-like regions exhibited a turnover rate of 3–4 days (n=5). The white contour lines indicate the crypt regions. Scale bar, 100 μm. (G) The area of villus regions was quantified daily. The error bars denote standard deviation.

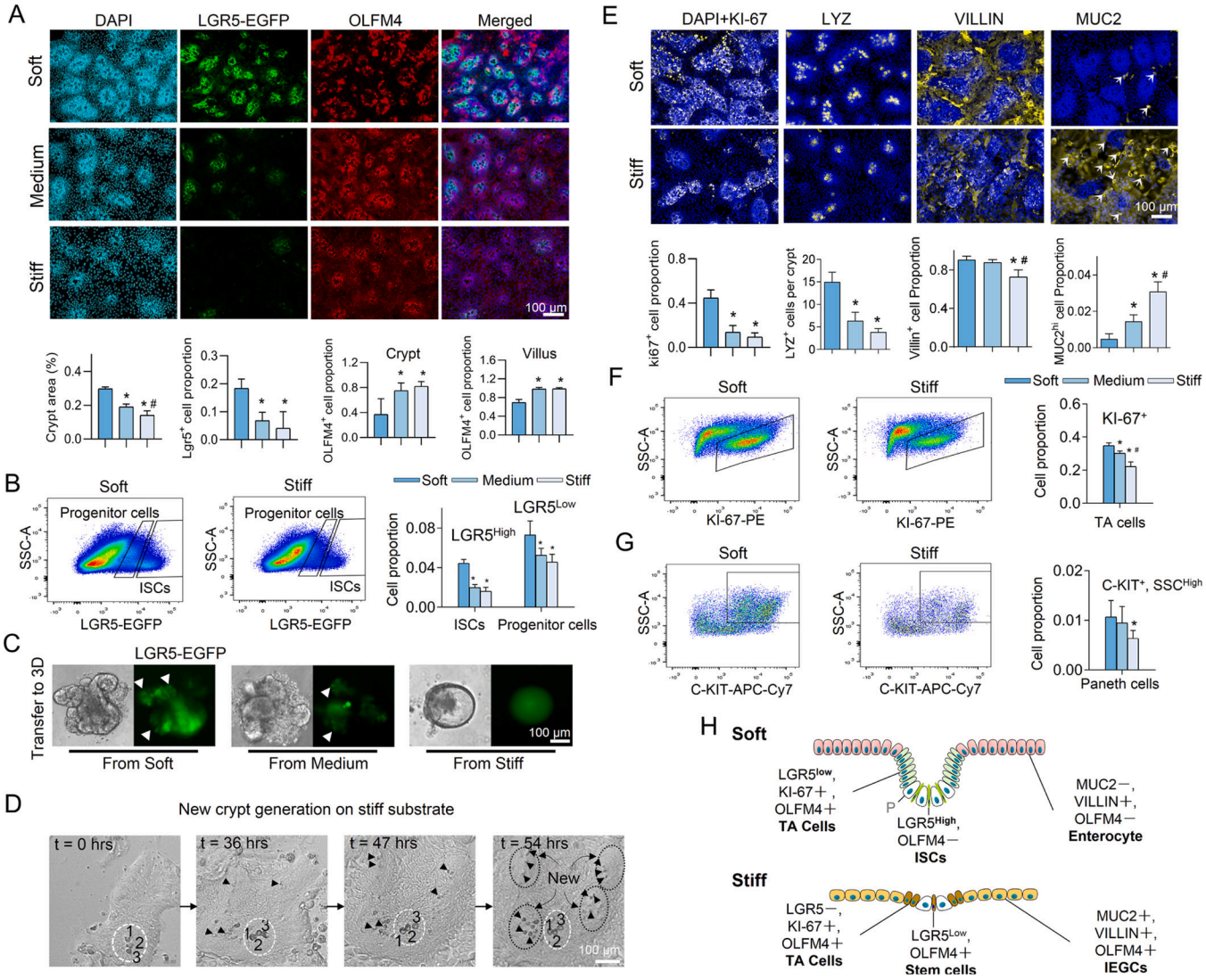

Figure 2. Stiffness determines the fate of ISCs.

(A) Increasing the matrix stiffness from soft (0.6kPa) to medium (2.4kPa) to stiff (9.6kPa) reduced the size of the crypt-like regions with dense nuclei and decreased the expression of LGR5. Stiffening also extended the OLFM4^{+} cells into villus-like regions. Scale bar, 100 μm. The crypt surface area was quantified as a proportion of total area, the number of LGR5^{+} cells as a proportion of total cells, and the number of OLFM4^{+} cells as a proportion of total cells in the crypt regions and in the villus regions. (n=3–5). (B) Flow cytometry analysis showed that stiffening decreased LGR5^{high} ISCs and LGR5^{low} progenitor cells (n=3). (C) The 3D organoids derived from the soft and medium matrix budded with LGR5-EGFP^{+} ISCs (white arrows). The 3D organoids derived from the stiff matrix grew more like LGR5-EGFP^{-} cysts (n=3). Scale bar, 100 μm. (D) Live-cell imaging demonstrates the generation of new crypts in the villus-like region of the stiff substrate (Movie S2). At t=0 hrs, only one crypt is visible (labeled with a white dashed ellipse) surrounded by the villus region. The large and optically dark Paneth cells (enumerated by 1, 2 and 3) are used as a point of reference. At t=36 hrs, new Paneth cells (marked by black arrows) appear within

the villus region. At t=47 hrs, more Paneth cells are visible within newly formed crypts. At *t*=54 hrs, four new, fully formed crypts (labeled with black dashed ellipses) are visible. Scale bar, 100 μm. (E) Stiffening decreased the expression of KI-67, LYZ, and VILLIN, but increased MUC2 (*n*=3–5). Scale bar, 100 μm. KI-67^{+}, and VILLIN^{+} cells, and MUC2^{high} cells (indicated by arrows) were respectively quantified as their proportion of total cells. LYZ^{+} cells is quantified as cell number per crypt. Flow cytometry analysis showed that stiffening decreased KI-67^{+} TA cells (F, *n*=3) and Paneth cells (G, *n*=6). (H) Schematic summarizing the impact of stiffening on all cell types. ‘P’, Paneth cell. * vs. Soft and # vs. Medium, $P<0.05$ (One-way ANOVA analysis). The error bars denote standard deviation.

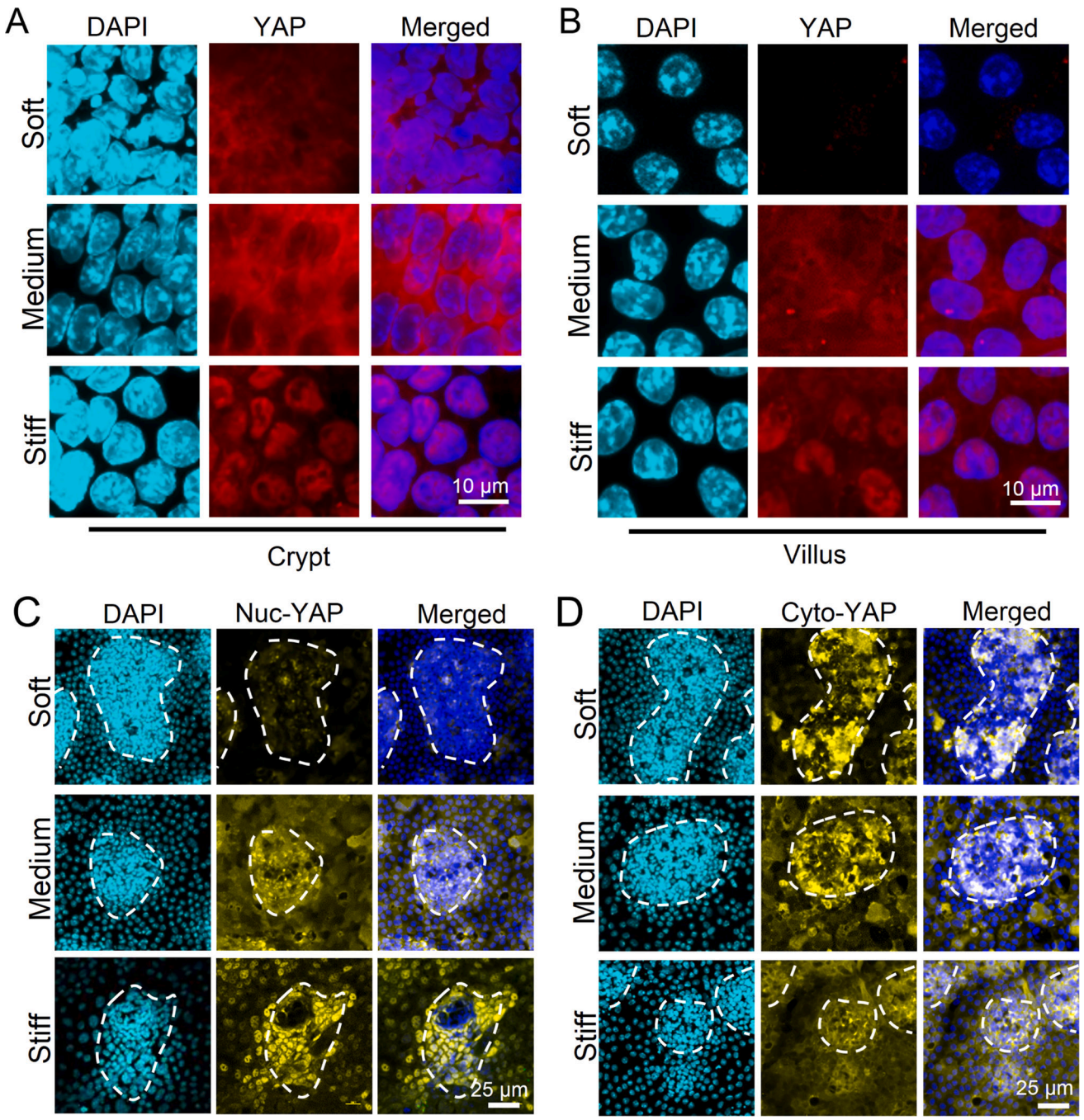

Figure 3. Influence of stiffness on YAP expression and sequestration in crypt-like and villus-like regions.

On the stiff gel, nuclear localization of YAP was shown on both crypt (A) and villus (B) regions. In villus regions, cyto-YAP expression was absent on the soft matrix and highly expressed on the medium matrix (B). (n=3). Scale bar in (A) and (B), 10 μm. (C) The non-phosphorylated nuclear (nuc-) YAP was increased by stiffening and showed clear nuclear localization on the stiff matrix (n=5). Scale bar, 25 μm. (D) The Ser 127 phosphorylated cytoplasmic (cyto-) YAP was decreased by stiffening in the crypt-like regions, but increased in the villus-like regions (n=5). Scale bar, 25 μm.

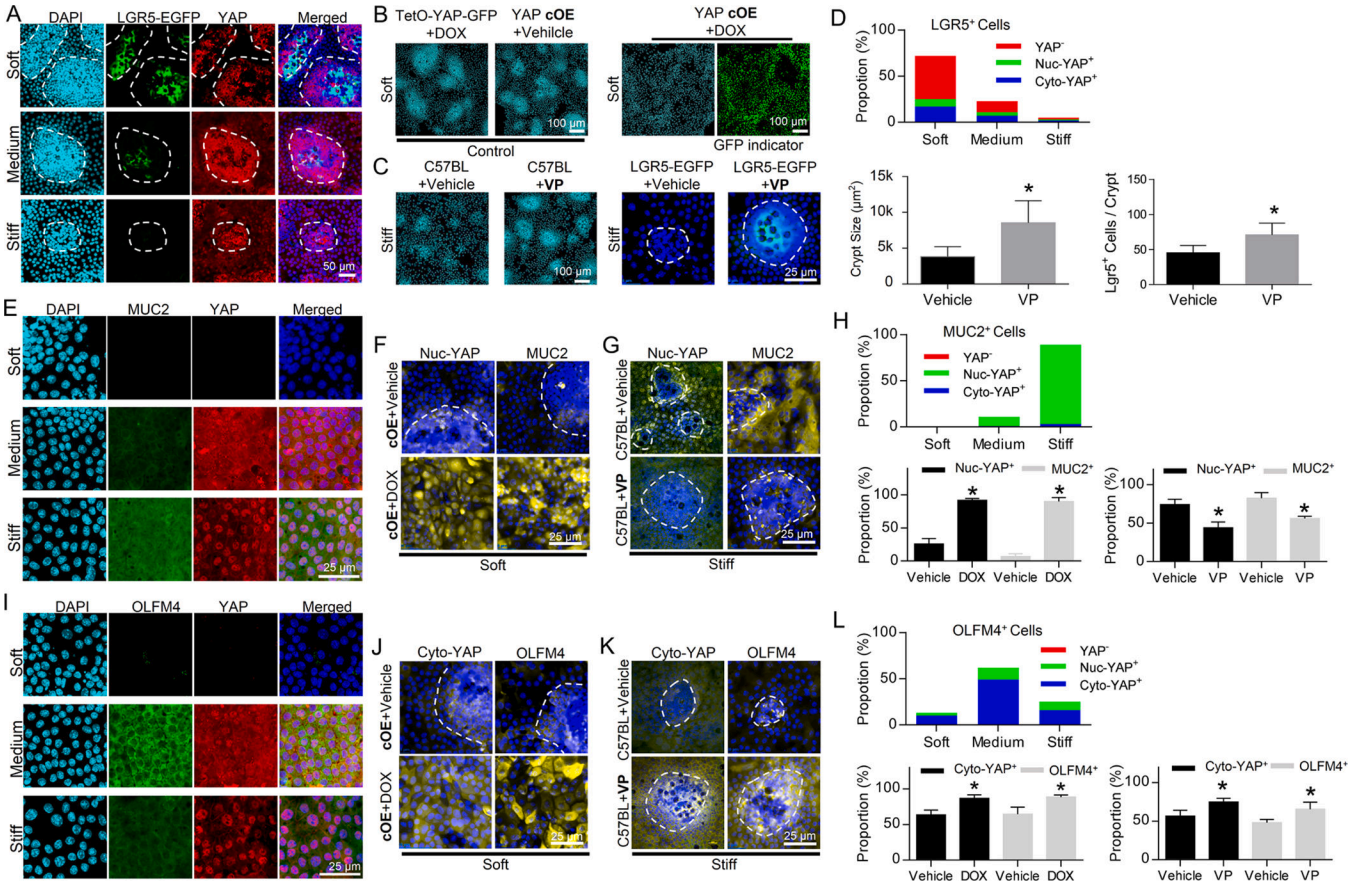

Figure. 4. Stiffness regulates ISC fate via YAP. The fate of ISCs was manipulated via conditional YAP knockout (cKO), conditional YAP overexpression (cOE), and Verteporfin (VP).

(A) Lgr5-EGFP^{+} ISCs were YAP^{-} and disappeared when YAP expression was positive. The white dashed lines trace the crypt-like regions (n=3). Scale bar, 50 μm. (B) YAP cOE led to the loss of the crypt-like regions on the soft matrix. TetO-YAP-GFP cells with DOX and YAP cOE cells without DOX served as control groups. Scale bar, 100 μm. (C) VP administration increased the size of the crypt-like regions and restored LGR5-EGFP expression on the stiff matrix. Scale bars, 100 μm for the C57BL mouse group and 25 μm for the LGR5-EGFP mouse group. (D) Quantification of (A, B and C) shows the proportions of YAP^{-}, nuc-YAP^{+} and cyto-YAP^{+} cells in LGR5^{+} cells as well as impacts of VP on crypt size and number of LGR5^{+} cells per crypt. (E) MUC2 was highly expressed in cells with intense YAP nuclear localization in villus regions (n=3). Scale bar, 25 μm. (F) YAP cOE on soft substrate increased both nuc-YAP and MUC2. Scale bar, 25 μm. (G) VP administration on stiff substrate decreased both nuc-YAP and MUC2. Scale bar, 25 μm. (H) Quantification of (E, F and G) shows the proportions of YAP^{-}, nuc-YAP^{+} and cyto-YAP^{+} cells in MUC2^{+} cells and the impacts of YAP OE and VP on the proportions of nuc-YAP^{+} and MUC2^{+} cells in total cells. (I) OLFM4 expression was highly correlated with cytoplasmic YAP stained with total YAP in villus regions (n=3). Scale bar, 25 μm. Both YAP cOE on soft substrate (J) and VP administration on stiff substrate (K) persistently increased cyto-YAP and OLFM4. Cyto-YAP was stained with Ser 127 phosphorylated YAP. Scale bar in (J) and (K), 25 μm. (L) Quantification of (I, J and K) shows that the proportions of YAP^{-}, nuc-YAP^{+} and

cyto-YAP^{+} cells in OLFM4^{+} cells and the impacts of YAP OE and VP on the proportions of cyto-YAP^{+} and OLFM4^{+} cells in total cells. *, $P<0.05$ (Student's *t*-test). The error bars denote standard deviation.

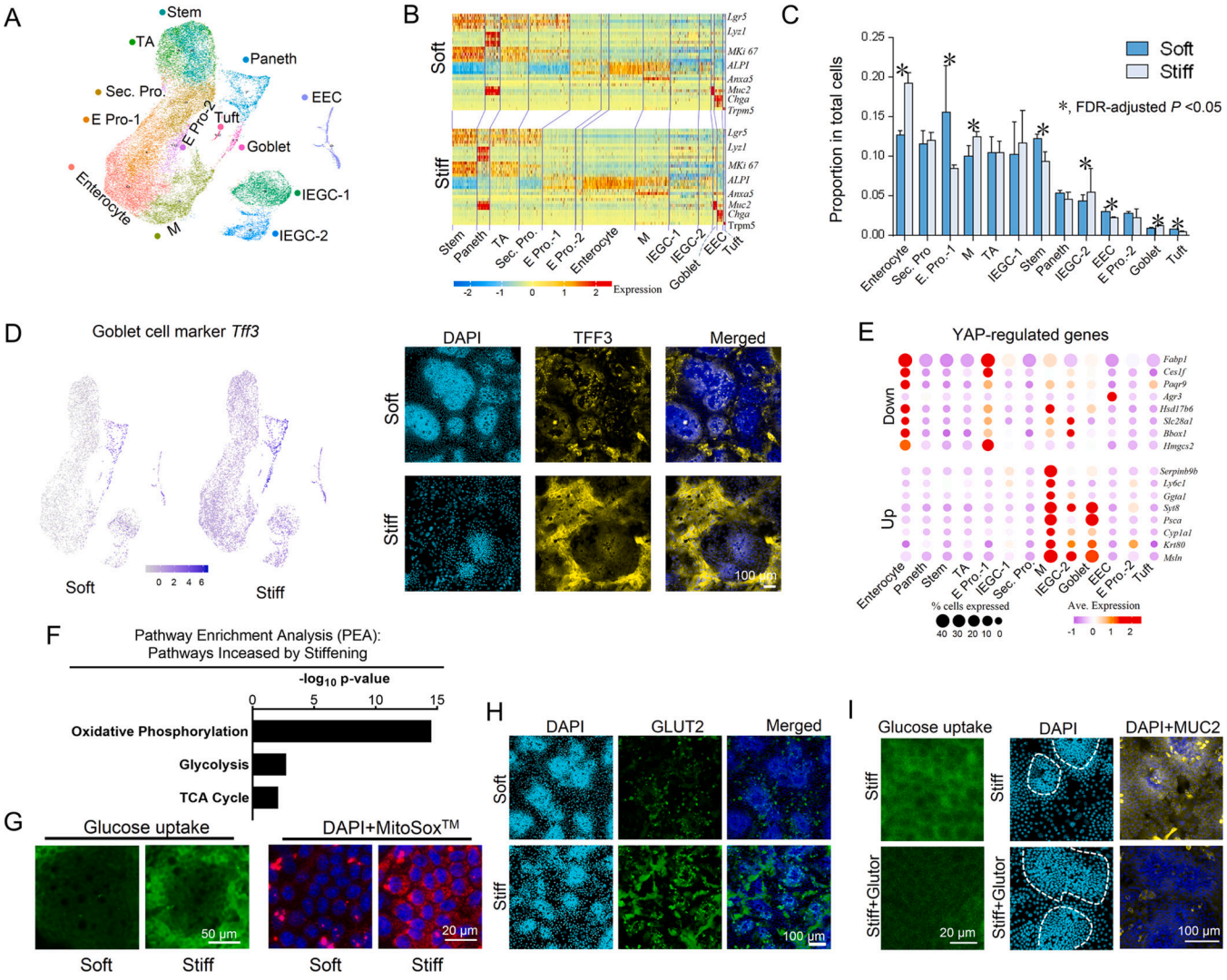

Figure 5. Single cell RNA sequencing of 2.5D gut organoids.

(A) UMAP plot with cell clusters (marked by color) including ISCs and differentiated cells. ‘Sec’, secretory; ‘Pro’, progenitor; ‘E’, enterocyte; ‘M’, microfold. (B) Heat map for marker genes of each cell type (Figure. S5). (C) The differences of the proportions of each cell type between the soft and stiff matrices analyzed using the scProportionTest tool. (D) Differential expression analysis and immunofluorescence showed that expression of *Tff3* gene was higher on the stiff matrix compared to the soft matrix. Scale bar, 100 μm. (E) Genes downregulated by YAP were highly expressed in the enterocyte and E pro-1 clusters; genes upregulated by YAP were highly expressed in goblet cells, IEGC-1, and M cells. (F) Pathway enrichment analysis (PEA) demonstrates that the metabolic pathways involved in glucose uptake and catabolism, including oxidative phosphorylation, glycolysis, and TCA cycle, are more enriched on the stiff substrate. (G) Glucose uptake and mitochondrial activity assays, using 2-NBDG Administration and Mitosox measurement, respectively, demonstrate that stiffening increases glucose uptake and catabolism. Scale bars, 50 μm for the glucose uptake images and 20 μm for the Mitosox images. (H) GLUT2 expression was greater on stiff matrix compared to soft matrix. Scale bar, 100 μm. (I) On stiff matrix, the

administration of the pan-class I GLUT inhibitor, Glutor, inhibited the uptake of glucose analog 2-NBDG, increased the crypt size, and decreased MUC2 expression. Scale bars, 20 μm for the glucose uptake images and 100 μm for the MUC2 staining images. n=3 for A-I.

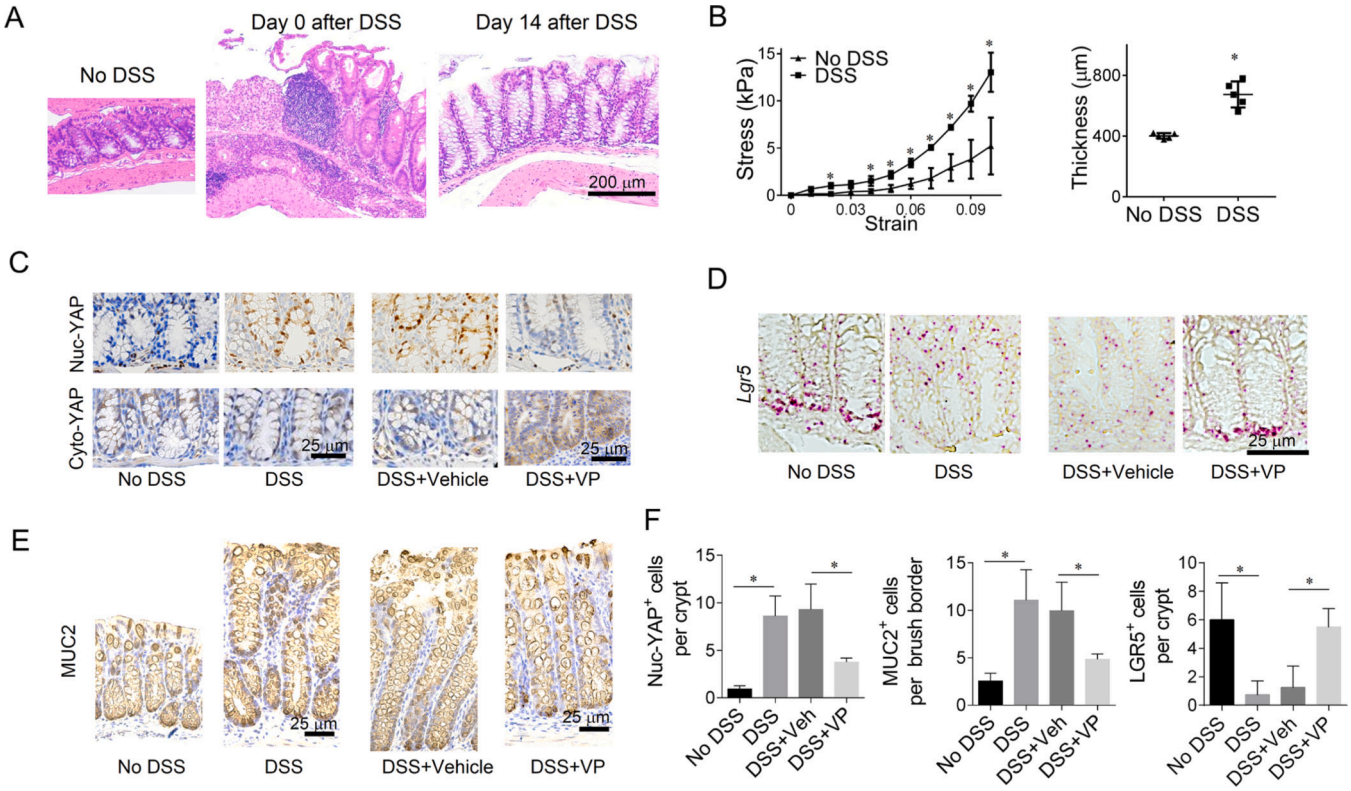

Figure 6. Stiffness regulates ISC fate in chronic colitis mouse model.

(A) H&E staining shows that the colon epithelium with severe damage on Day 0 was significantly regenerated on Day 14. Scale bars, 200 μm. (B) Colon stiffened (n=3) and thickened (n=6) in the DSS-induced colitis group compared with the control group without DSS. Methods for the Measurement of colon stiffness and thickness are in Method. (C) As shown in immunohistochemistry (IHC), nuc-YAP stained with non-phosphorylated YAP increased in the DSS groups compared with No DSS control. VP treatment caused a reduction of nuc-YAP and increased cyto-YAP expression. Scale bars, 25 μm. (D) In situ hybridization (ISH) showed that *Lgr5* expression was suppressed in DSS ground and was recovered after VP treatment. Scale bars, 25 μm. (E) MUC2 expression (IHC) was augmented in colon brush border of DSS groups, and was decreased after VP administration. Scale bars, 25 μm. (F) Quantification of nuc-YAP$^+$ cells and LGR5$^+$ cells per crypt and MUC2$^+$ cells per colon brush border. n=3–6. *, P<0.05 (Student's t-test). The error bars denote standard deviation.

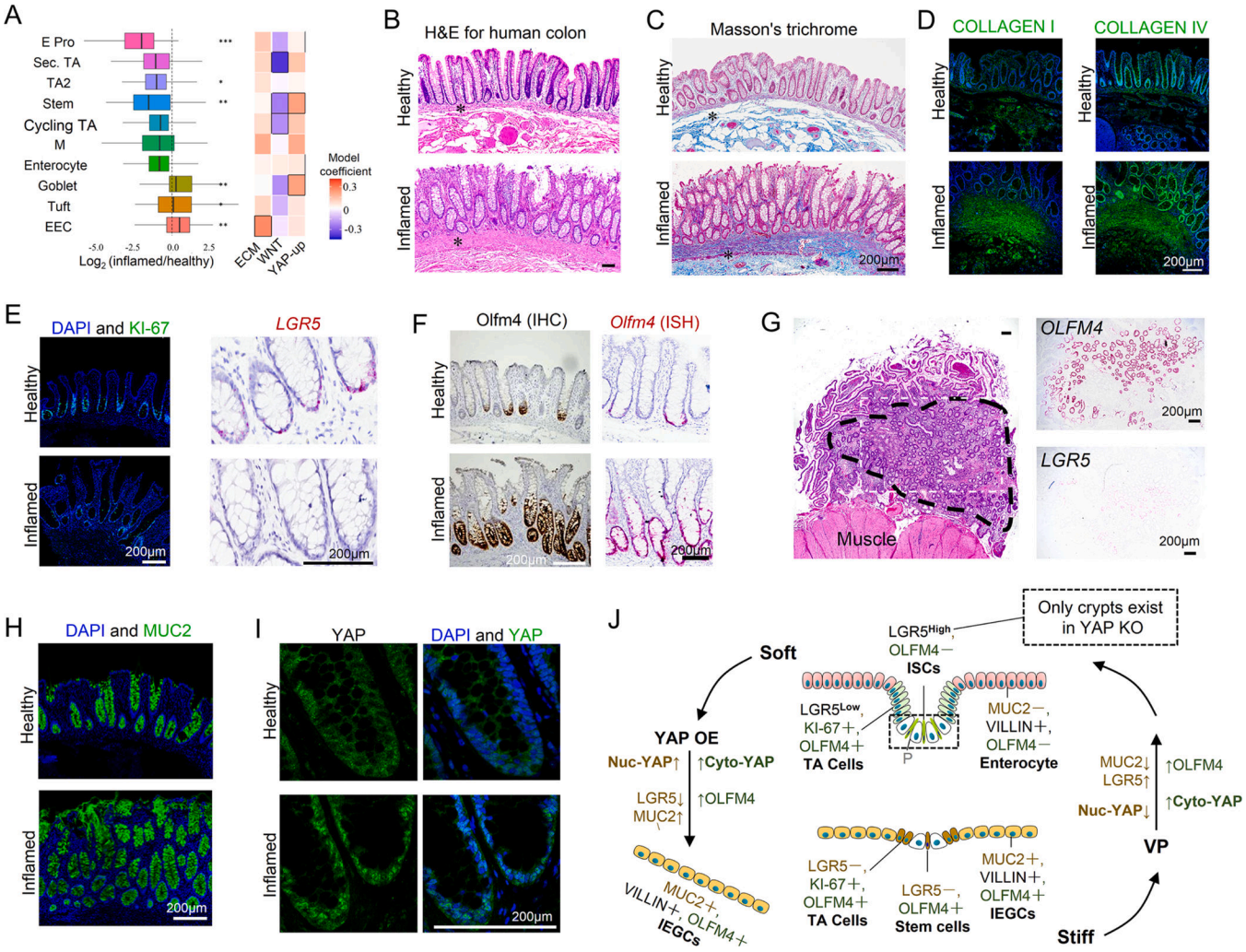

Figure 7. Stiffness regulates ISC fate in human IBD patients.

(A) scRNAseq analysis showed a decrease in ISC population and an increase of goblet cell population in human IBD colon. **P*<0.05, ***P*<0.01, ****P*<0.001. Pathway enrichment analysis showed that in IBD samples, *WNT* signaling is suppressed in ISCs, YAP up-regulated genes are highly expressed in ISCs and goblet cells, and ECM biosynthesis is activated in EECs. Boxes outlined in Black represent *P*<0.05 for the linear mixed model and *P*<0.05 for pathway enrichment (Method). (B) H&E staining of human colon tissues shows thickening of the BM and lamina propria (labelled with asterisks). Masson's trichrome staining (C) and staining of COLLAGEN I and IV (D) reveal fibrosis of lamina propria. Scale bars in (C) and (D), 200 μm. (E) KI-67^{+} proliferating cells and LGR5^{+} ISCs were decreased, and (F) OLFM4^{+} cells were increased in the IBD samples. Scale bars in (E) and (F), 200 μm. (G) In a large area (outside the dashed line) of the strictured ileum (extreme fibrosis), the invaginated ISC niche-crypts nearly disappear and only pieces of the villi remain. Numerous ectopic crypts (inside black dashed line) have formed and expressed strong OLFM4 and weak LGR5. Scale bar, 200 μm. (H) MUC2+ goblet cells increased in the inflamed colon. (I) YAP showed greater expression and nuclear localization in the IBD colon. *n*=6. Scale bar, 200 μm. (J) Schematic describing the stiffening-dependent ISC fate,

showing that stiffness regulates ISC fate via YAP, and YAP OE transforms the soft-matrix phenotypes into the stiff-matrix phenotypes, and VP does the reverse. ‘Yellow’ indicates regulation by nuc-YAP. ‘Green’, regulation by cyto-YAP.